

UNIVERSITY of CALIFORNIA
SANTA CRUZ

**SEARCH FOR TRAP RELEASE EFFECTS IN IRRADIATED
SILICON DIODE SENSORS**

A thesis submitted in partial satisfaction of the
requirements for the degree of

BACHELOR OF SCIENCE

in

PHYSICS

by

Jane Gunnell

1 June 2018

The thesis of Jane Gunnell is approved by:

Bruce A Schumm
Advisor

David Smith
Theses Coordinator

Robert P Johnson
Chair, Department of Physics

Copyright © by

Jane Gunnell

2018

Abstract

Search for Trap Release Effects in Irradiated Silicon Diode Sensors

by

Jane Gunnell

The international Linear accelerator is a proposed particle accelerator that will collide electrons and positrons in northern Japan. It hopes to unlock some of the mysteries that still surround the Standard Model of Particle Physics. The T-506 group at the Santa Cruz Institute for Particle Physics is working on testing sensors of different solid-state materials to see how well they withstand radiation in order to be used in the forward most calorimeter at the ILC. T-506 has recently taken on the task of searching for effects from the release of trapped charges, which is the main subject of this thesis. By changing the amount of time a signal is collected for a electron-hole pair created by passing minimum-ionizing particles, it may be possible to observe an increase in collected charge with collection times, indicating the charge that was trapped in an irradiated sensor has tunneled out. Six collection times were chosen to be studied. There was no loss of charge collection observed for collection times as short as 64ns. We concluded there may have been some indication of trapped charges exiting the sensor in the largest collection time, $4.2\mu s$, indicating the trap release time may be on the order of a few microseconds. Further tests are needed to see if this effect is truly being seen.

Contents

List of Figures	v
List of Tables	vi
Acknowledgements	vii
1 Introduction	1
1.1 The International Linear Collider	2
1.2 T-506 Radiation Damage Studies	4
1.3 Trapped Charges	6
2 Apparatus	8
2.1 Collection Time Circuitry	9
3 Collection Time	10
4 Signal Acquisition and Calibration	15
4.1 Data Acquisition Script	15
4.2 Calibration	17
4.3 Error Analysis	18
5 Analysis of WSI-P4 Charge Collection	23
5.1 CCE with WSI-P4	23
5.2 Results	24
5.3 Error Analysis	26
6 Conclusion	29
7 Bibliography	31

List of Figures

1.1	The Beamcal Diagram	3
2.1	Apparatus	9
3.1	10nf Integrator and Differentiator Pulse Shape	12
3.2	1nf Integrator and Differentiator Pulse Shape	12
3.3	Collection Time Python Output	13
4.1	Average Waveform of Sensor Signal Output	16
4.2	Histogram of Sensor Signal Output	16
4.3	Python Analysis Output	17
4.4	Histogram of Nominal Gain Configuration for the 4150ns Collection Time for Gain Calculation	19
4.5	Histogram of Nominal Gain Configuration for the 4150ns Collection Time for Gain Calculation	20
4.6	Histogram of Shifted landau Fit for 4150ns Collection Time for Gain Calculation	20
4.7	Histogram of Shifted landau Fit for 4150ns Collection Time for Gain Calculation	21
4.8	Histogram of Shifted landau Fit for 4150ns Collection Time for Gain Calculation	22
5.1	Log Plot of WSI-P4 Collection Time Data	24
5.2	Log Plot of WSI-P4 Collection Time Data, Scaled	25
5.3	Histogram of Nominal Landau Fit of WSI-P4 at 800V for the 64ns Collection Time	27
5.4	Histogram of Left Shifted Landau Fit of WSI-P4 at 800V for the 64ns Collection Time	28
5.5	Histogram of Left Shifted Landau Fit of WSI-P4 at 800V for the 64ns Collection Time	28

List of Tables

3.1	Integrator and Differentiator with associated Collection Time	14
4.1	Collection Times and their associated gains	18
5.1	Median Voltages and Charges and their associated gains for given collection times	24

Acknowledgements

I would like to thank Bruce Schumm for this opportunity, as well as his help and support while working at T-506. I would also like to thank all the members of T-506 past and present who made this thesis possible, and all the members at SCIPP who have helped me along the way.

and

I would like to thank my family for making it possible for me to be here and being unconditionally supportive.

1

Introduction

The current Standard Model of particle physics is a great foundation for the field, but in and of itself cannot provide a self-consistent model of nature at all energy scales. The International Linear Collider (ILC) is a proposed linear electron-positron collider currently under design that will likely be imperative to the development of the Standard Model and beyond. In large particle accelerators such as the ILC, radiation damage degrading the performance of the particle detectors is an issue that needs to be addressed, particularly for detectors mounted close to the incoming and exiting beams. In association with the SLAC National Accelerator Laboratory, the T-506 group at the Santa Cruz Institute for Particle Physics (SCIPP) is testing the radiation hardness properties of Silicon (Si), Gallium Arsenide (GaAs), Silicon Carbide (SiC), and Sapphire (Al_2O_3) sensors to be used in the design of the forward most calorimeter of the particle detectors at the ILC. In this thesis, I report on a study attempting to look for the effects of the release of trapped charges in a silicon

diode sensor that has been irradiated by the T-506 group.

1.1 The International Linear Collider

The ILCs most likely site of the ILC is Northern Japan. It will stretch approximately 31 km and collide beams of electrons and positrons with an energy scale of about 500 GeV (Behnke, Ties et. al 2007).

To date there has been only one major linear collider in existence, the Stanford Linear Accelerator. This accelerator was 3.2 km long, with a beam energy of up to 50 GeV (Richter et al. 1980, Erickson et al. 1984) and in the 1990s it was integral to exploring the Z boson. The ILC is a much higher energy particle accelerator with a much higher event rate than the Stanford Linear Accelerator, allowing ILC to create a wider range of particles to be studied, in particular the Higgs Boson.

There already exists a high energy particle accelerator called the Large Hadron Collider (LHC) that collides hadrons in Switzerland. The advantage of the ILC is its increased accuracy and precision compared to the LHC (Weiglein, G. 2005). The ILC achieves this accuracy and precision by colliding electrons and positrons which are much easier to analyze than collisions of hadrons. Hadrons are composed of quarks and gluons, so the energy of a hadron is distributed among these composite particles. Conversely, electrons and positrons are fundamental particles and are composed of nothing but themselves. Because the initial state of the colliding particles are thus precisely known, the ILC allows for precision measurements of particle properties.

For the collision point of the ILC two particle detectors are being designed, the Silicon Detector (SiD), and the International Large Detector (ILD) (Brau, James et. al 2007). Particle detectors are made up of many parts, including several calorimeters that measure the energy of particles. The most forward part of the SiD and ILD is the Beamline Calorimeter (BeamCal), as seen in figure 1.1, a calorimeter made up of solid-state sensors sandwiched between plates of tungsten. Tungsten is used because its high density produces very collimated showers of photons, electron, or positrons. The Beamcal is located about three meters on either side of the collision point and covers a region between 5 and 50 milliradians measured from the beam axis. The Beamcal receives the brunt of the electromagnetically induced radiation from the collisions of the beams of electrons and positrons with an estimated radiation dose of 100 Mrad a year at its peak. Radiation damage results in degradation of detector performance and given the radiation dose the BeamCal is expected to receive, it is imperative that the sensors be constructed from a technology that can withstand high radiation doses.

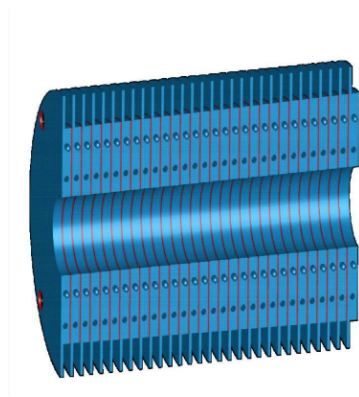


Figure 1.1: A cross sectional diagram of the beamcal. The red strips are the solid state detectors, while the blue strips are the tungsten

1.2 T-506 Radiation Damage Studies

Radiation damage is a well documented effect, from the work of Chisaka (1973) on radiation damage in silicon nuclear detectors to the study of Matthews et al. (1996) on radiation damage of silicon detectors at the LHC. As accelerators become higher energy and more intense, radiation damage has become more and more of a concern, leading many groups to put work into finding radiation-hard materials to be used in particle detectors.

Silicon is the most studied and used semiconductor material used in particle detectors. Silicon is desirable for a few reasons: it has good temperature stability, large forward current, low leakage current, high reverse breakdown voltage, and it has a very low cost (Atlas Inner Detector Community, 1997).

To assess radiation hardness there are two parameters of interest: charge collection efficiency (CCE) and leakage current (IV), both of which depend on the bias voltage applied to the sensor. CCE is a measurement of median charge collected from a sensor after the passage of a high energy particle. Once a sensor is irradiated, it becomes damaged and charge can get trapped within the sensor. This charge is then not recorded in CCE measurements, and the median charge collected decreases. IV is a measurement of leakage current drawn from the sensor. Leakage current leads to heat dissipated by the sensors, and this heat will need to be drawn away during the operation of the BeamCal. A contender for a radiation hard sensor would show little degradation in median charge after irradiation and have an acceptably low leakage

current. CCE and IV data are taken pre and post irradiation to test the radiation effects on the material.

For the T-506 project, irradiation takes place at SLAC's End Station A Test Beam (ESTB) facility where the sensor is placed in the electron beamline. There are three tungsten plates, one directly in front of the sensor, one a half a meter in front of the sensor, and one directly behind the sensor. Details can be found in Anderson et al. (2016), Updated Results of a Solid-State Sensor Irradiation Study for ILC Extreme Forward Calorimetry.

Updated Results of a Solid-State Sensor Irradiation Study for ILC Extreme Forward Calorimetry.

The first two plates ensure the electromagnetic shower is at a maximum at the sensor, creating a high radiation environment, while the plate behind the sensor absorbs the shower. By surrounding the sensor with tungsten, the conditions in which the beamcal will be operated at the ILC are replicated. Specifically, the sensor is exposed to a realistic dose of neutrons, which are emitted by nuclei that absorb γ rays in the shower. The sensor is then taken back to SCIPP to analyze.

Once CCE and IV data are taken for a freshly irradiated sensor, we can attempt to reverse radiation by annealing a sensor. Annealing refers to controlled heat treating of the sensor causing thermal vibrations that allow atoms to migrate in the crystalline structure, undoing some of the radiation damage (Fleischer, R. L. et al. 1964). For our purposes, we anneal a sensor by simply keeping it at the desired temperature for an hour. Sensors are annealed in steps ranging from room temperature to 100°C. CCE

and IV data are taken at each annealing step. Comparison of the pre-anneal, post anneal, and pre-irradiated data is done to determine if annealing had any benefits to median charge restoration and leakage current. We can then determine if the sensor material is a good candidate for a radiation hard material.

1.3 Trapped Charges

In addition to radiation hardness studies, the T-506 group recently started analyzing trapped charges inside irradiated sensors which will be the subject of this thesis. One of the ways in which radiation damage manifests in solid state devices is called bulk damage (Junkes, Alexandra 2011). Bulk damage occurs when atoms are displaced from lattice sites in the crystalline structure of the material.

The first atom to be displaced is called the primary knock on atom (PKA). As the PKA moves through the material it will lose energy to ionization and from collisions with other atoms in the lattice. Some of these atoms will be knocked out of the crystalline structure and become interstitial, i.e. settle into a spot outside of the lattice sites in the crystal structure. Eventually, the PKA will stop moving and also become interstitial. At this point non-ionizing interactions between the PKA and the other atoms in the structure result in what is called a cluster defect. Cluster defects cause an intermediate state in the bandgap to form. It is possible for charges from particles to be trapped in this intermediate state, with a possibility of eventually getting released and tunneling out.

The amount of time data is collected for a given pulse is called the shaping time. Shaping time is related to the amount of time it takes for a pulse to rise or fall between 10% and 90% of its maximum value. If charges are trapped for longer than this shaping time a loss of CCE will result. In this project, signal length is characterized by a quantity called "collection time", which is closely related to rise and fall time. The definition and motivation for collection time will be given in chapter 3. T-506 has taken on the task of trying to measure the amount of time it takes for a particle to be trapped and subsequently release, a phenomena called the trap release time, through observing the CCE as a function of charge collection time.

In this work we made use of a p-bulk silicon diode sensor called WSI-P4. WSI-P4 was chosen because it is a good candidate for the beamcal semiconductor material. This sensor has been irradiated to 570Mrad, well above the expected 100Mrad yearly dose the Beamcal is expected to receive, and its median charge is above 50% of the pre-irradiated median charge at 600V. IV tests on the WSI-P4 sensor suggest that when operated at -30° , a Beamcal constructed of such sensors would produce a yearly addition to the beamcal power draw of less than 20W.

This thesis will discuss the particulars of the CCE apparatus and how it is used to try and explore the trap release times in irradiated silicon.

2

Apparatus

As discussed above, we are interested in observing median charge as a function of collection time. In order to achieve this, we need to use the CCE apparatus that sits inside a freezer at SCIPP. The apparatus is contained within a freezer so it can be kept at sub-zero temperatures in order to avoid annealing effects during IV and CCE measurements. Within the freezer there is a strontium-90 source that decays into a β -particle and Yttrium 90, which emits another β -particle of energy 2.28MeV. This second β -particle is directed through a sensor mounted on a daughter board. The sensor is connected to an low noise pre-amplifier designed at SCIPP specifically for a project to explore varying collection times by a former member of T-506, which is mounted close by the daughter board. The β -particles pass through the sensor hitting a scintillator positioned behind it. The scintillator absorbs β -particles and emits a light signal which is then sent through a photo multiplier tube, triggering a Tektronix DPO 4054 Oscilloscope. Charged deposited onto the sensor from the beta particles is

converted into a voltage signal using the amplifier board powered by a BK Precision 1760A DC Power Supply. This signal is sent through a Sonoma Instrument 310 SDI amplifier to further amplify the signal, which is then displayed on the oscilloscope. Bias Voltage to the sensor is provided by a Keithley 237 High Voltage Supply. A schematic of the components inside the freezer is given in figure 2.1.

2.1 Collection Time Circuitry

In order to adjust the collection time of the signal two Pomona Boxes holding capacitors and resistors are used. A high pass filter called a differentiator is placed before the SDI amplifier, which holds one capacitor in series, while a low pass filter called an integrator, that has a series 50Ω resistor with a capacitor to ground, is placed directly after the SDI amplifier. The resistor in every integrator is 50Ω , but changing the capacitors inside these filters allows us to alter the collection time.

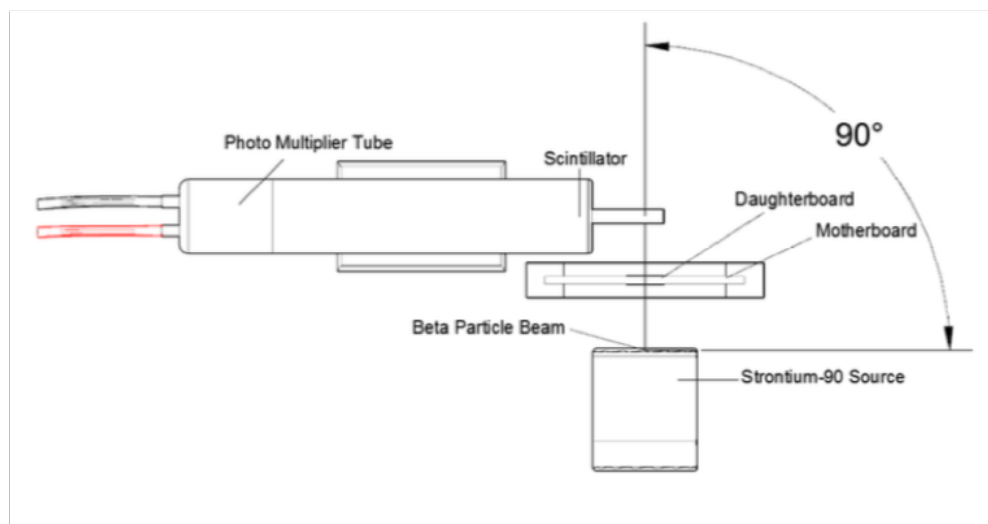


Figure 2.1: Components of CCE apparatus inside freezer

3

Collection Time

In order to classify shaping time, we defined something called the collection time. The collection time is the time separation between two identical signals that when added together yield a combined signal with the 1.5 the maximum height of each individual signal. This was simply chosen as a way to categorize the length of time the electronics collected charge. A thin pulse has a shorter collection time and vice-versa.

Collection time is the crux of this thesis because it is what allows us to study the trap release effect. The more conventional shaping time is related to the rise or fall between 10% and 90% of its maximum value. Therefore if all the pulses' were completely symmetric, shaping time would be a fine definition. The asymmetry of the pulses rise and fall time calls for another way for these pulses to be categorized.

When picking collection times for this study, a few motivations were kept in mind. First, there needed to be a large range of collection times, over multiple orders, that

needed to be studied in order to get a full picture of how the trap release time is effected by different pulse lengths. Second, although asymmetry of the pulses was why collection time needed to be defined in the first place, it was best if the pulses were relatively symmetric. Lastly, it is more desirable if signal to noise ratio is low. For reasons still not understood, at the highest and lowest collection times, the signal to noise ratio was very high, resulting in a large uncertainty in the final results for these collection times. More studies need to be done to fully understand this effect, and potentially extend the study to shorter or larger collection times.

In order to determine collection time for a given integrator and differentiator, or collection time configuration, a LeCroy pulse generator 9210 was set to a step function response. This signal was injected directly into the front of the pre-amplifier via a calibration capacitor. The differentiator follows the pre-amplifier, which is then followed by the SDI amplifier, integrator, and the oscilloscope. The collection time was manipulated by changing the integrators and differentiators. Figure 3.1 and 3.2 show the oscilloscope display for two different collection configurations.

The amplified pulse was acquired from the oscilloscope in the form of a CVS file and read into a python script. This code is available on the T-506 computer in SCIPP, inside the shaping time folder and is titled "Collection Time". The script made two copies of the waveform, one which stood still and one that stepped though increasing time offsets until the combined pulse height was 1.5 the original height. If the pulses were exactly on top of each other, the maximum of the combined pulse would be 2 times the original; if the pulses were completely separate the maximum

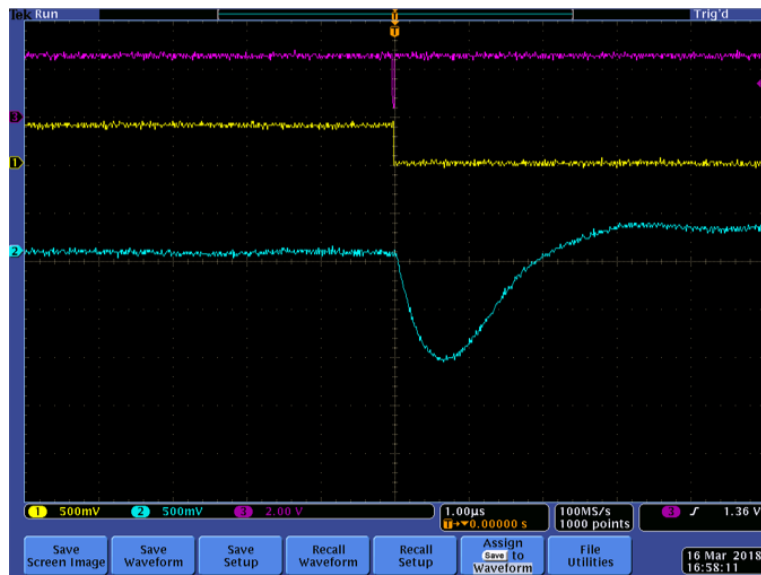


Figure 3.1: Picture taken from oscilloscope when integrator and differentiator with 10nf capacitors were in place, providing a 630ns collection time. The pink signal is pulse generator trigger, yellow signal is the step function from the function generator, blue channel is the resulting amplified signal

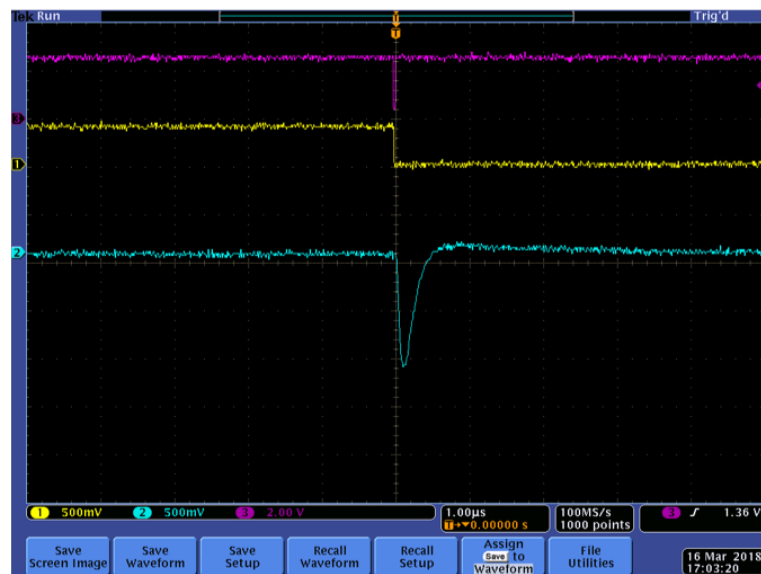


Figure 3.2: Picture taken from oscilloscope when integrator and differentiator with 1nf capacitors were in place, providing a 120ns collection time. The pink signal is pulse generator trigger, yellow signal is the step function from the function generator, blue channel is the resulting amplified signal

of the combined pulse would simple be one times the original pulse. Only when they are somewhat overlapped will you get 1.5 times height of the original pulse. The longer the width of the pulse, the longer it takes to reach that 1.5 height, resulting in a longer collection time. Conversely, if the pulses are narrow, it will not take very long to reach 1.5 the original height, resulting in a short collection time. The distance between the peaks of the two pulses is collection time, which is printed out at the bottom of the script. Figure 3.3 is an example of the code graph and output.

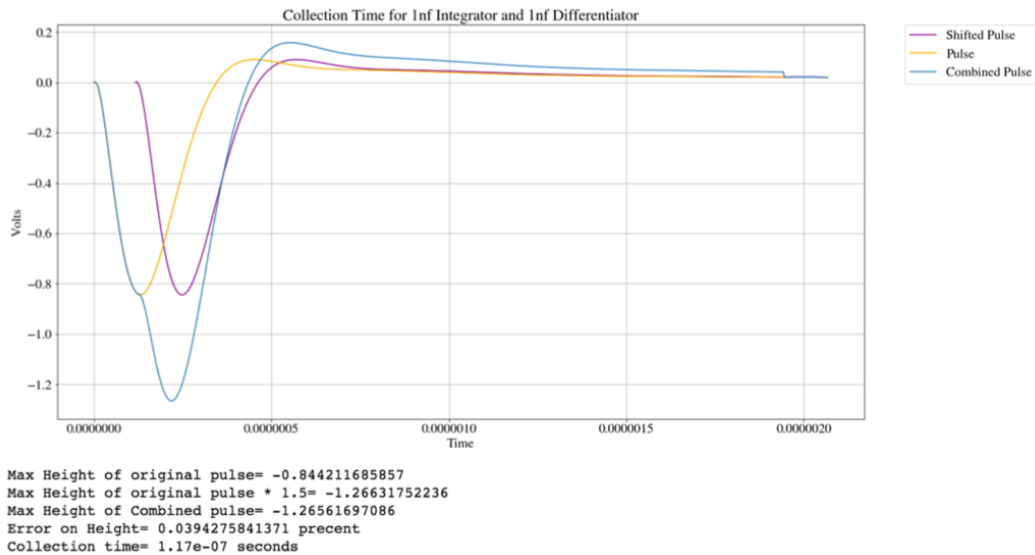


Figure 3.3: Example of the output from the python script used to find collection time for the configuration with 1nf differentiator and integrator boxes

This method was performed on all combinations of differentiator and integrator of which there were sixty-four options. The six collection times that were ultimately chosen are displayed in table 3.1.

Table 3.1: Integrator and Differentiator with associated Collection Time

Integrator	Differentiator	Collection Time(ns)
200pf	200pf	64
1nf	1nf	120
51pf	10nf	340
10nf	10nf	630
1nf	100nf	1080
100nf	100nf	4150

4

Signal Acquisition and Calibration

4.1 Data Acquisition Script

A given sensor's output signal from a particle passing through it appears as a wave form on the oscilloscope. These wave forms are captured by a python script on a nearby computer using a data acquisition program written by former T-506 members. The program deletes any duplicate wave forms and displays an average wave form of all wave forms captured as in figure 4.1.

The voltage at the time of the peak is recorded for each waveform, converted into femto-coulombs using the gain of the amplifier system, and a histogram of found charge is created as in figure 4.2.

The histogram has two components: a Landau distribution, which is the distribution of charge collected by the sensor, and a Gaussian that represents the noise of the system, arising from particles that missed the sensor but still hit the scintillator. A

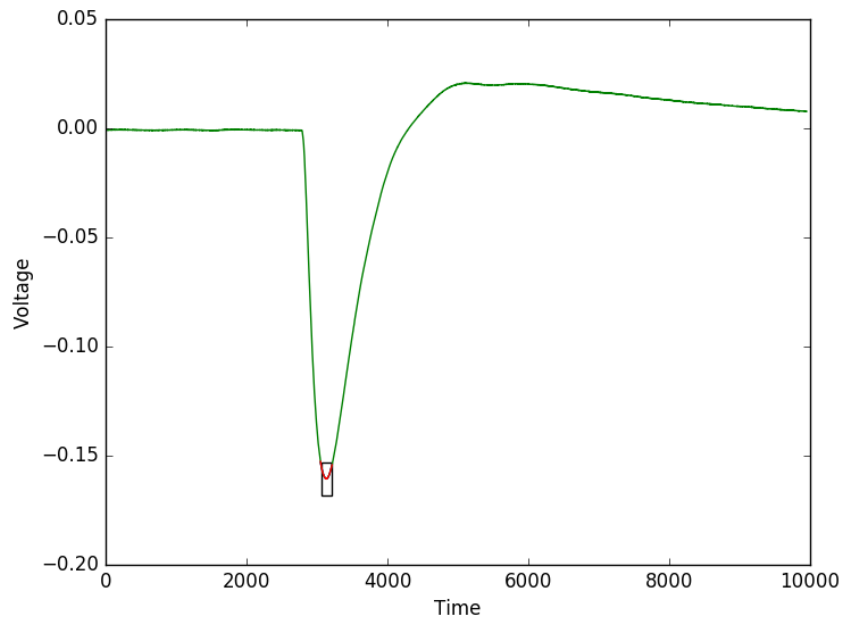


Figure 4.1: Average waveform for the un-irradiated N-type sensor silicon sensor run at 150V

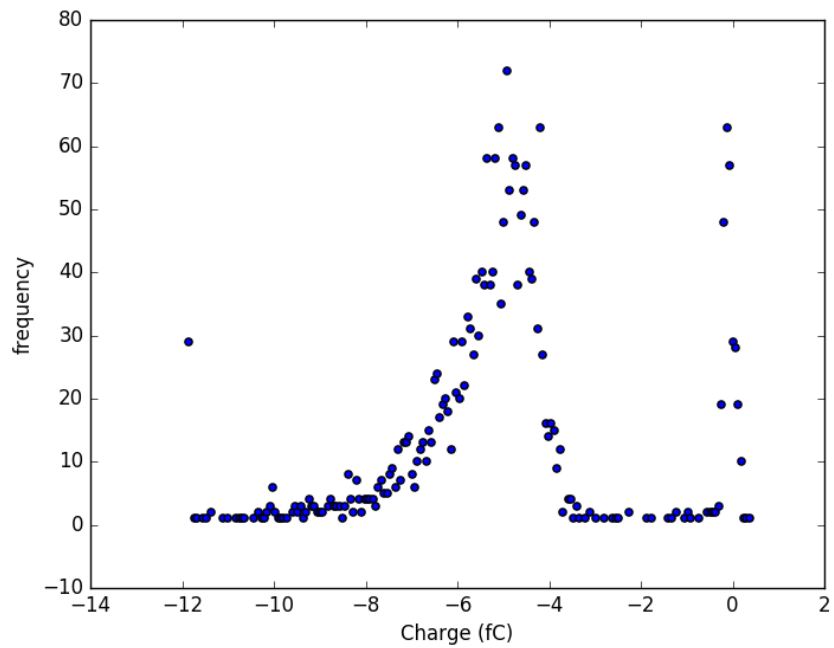


Figure 4.2: Histogram of the charge distribution of the particles triggering the photo multiplier tube for the un-irradiated N-type silicon sensor run at 150V

fit of the histogram is then performed by a python script written by a former T-506 member in which pre-specified parameter ranges for the Landau and Gaussian are input. The script returns the best fit for the parameters of the Gaussian and Landau distributions, including median collected charge, using a least squares fit algorithm. The error from the least squares fit is the same for every point, but the size of the statistical error is arbitrary, resulting in well fit parameters. Figure 4.3 shows the fit superimposed on the histogram of the charge collection data for a typical run of an un-irradiated sensor.

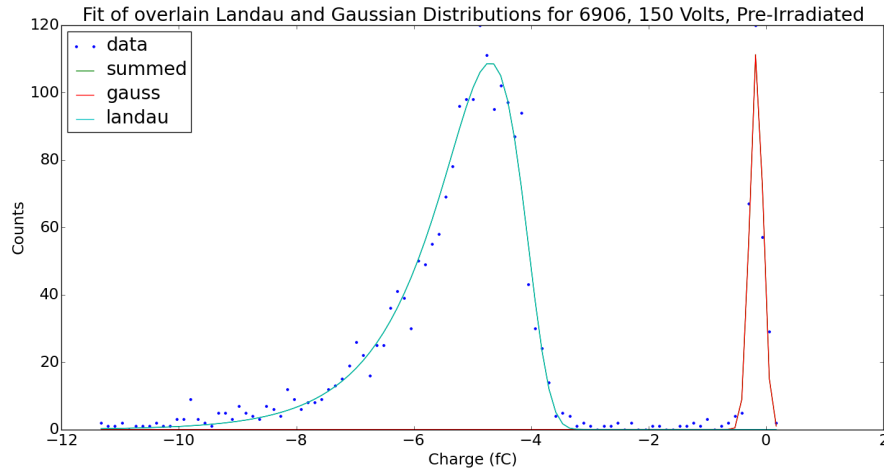


Figure 4.3: Python output of the analysis script that fits the Landau and Gaussian distribution of the un-irradiated N-type silicon sensor run at 150V and returns the median charge of the landau distribution

4.2 Calibration

The first step to collecting data for each collection time was determining the gains of each shaping time. The gain allows us to convert our voltage signal into a

measurable charge, but it changes when the capacitors in the integrators and differentiators are exchanged. To calibrate the gains of each collection time a well-studied un-irradiated n-type silicon sensor was placed in the CCE position, data was taken and analyzed to find the median charge. The gain was then adjusted until a median charged of 5.07fC was returned, which is the known median charge of this sensor. The gains for each collection time are given in table 4.1.

Table 4.1: Collection Times and their associated gains

Collection Time (ns)	Gain (V/fC)
64	2.06 \pm 3%
120	3.62 \pm 3%
340	11.3 \pm 3%
630	3.20 \pm 3%
1080	12.2 \pm 3%
4150	1.04 \pm 3%

These gains were used in all subsequent data analysis.

4.3 Error Analysis

Error analysis was done using the Landau and Gaussian fitting program described in section 4.1. The program calls for inputs such as height of the Gaussian, Landau, etc, in which a starting range for each of the landau and Gaussian parameters is input. The program then fits these parameters within the given range. One of the input parameters is the most probable value for the Landau distribution, which determines the position of the peak of the distribution. In order to find the error on a given median charge, the nominal most probable value was found for each collection

time, for both the runs with the calibration sensor as well as with the WSI-P4 sensor. The most probable value was then changed by hand by $\pm 5\%$ and then $\pm 10\%$, and the fit redone each time. These shifted graphs were then analyzed to determine what magnitude of a change in the most probable value could be tolerated by the data. Figures 4.4 through 4.8 show the the shifted Landau fits for the 4150ns calibration run.

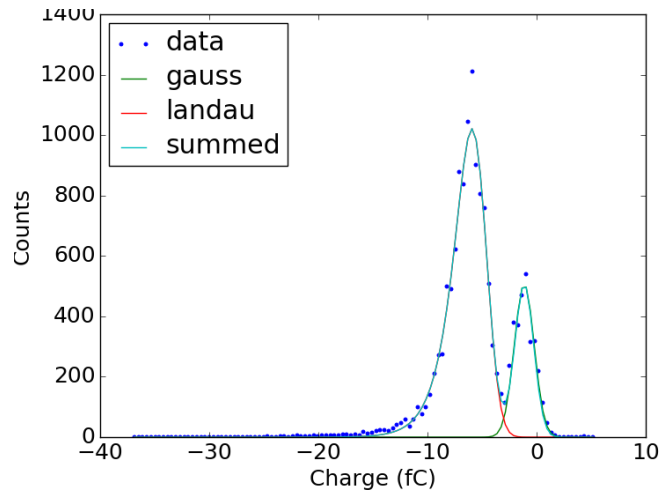


Figure 4.4: Nominal configuration of the histogram from CCE measurements using the well-studied silicon sensor with superimposed Landau and Gaussian fits to find the gain for the 4150ns collection time.

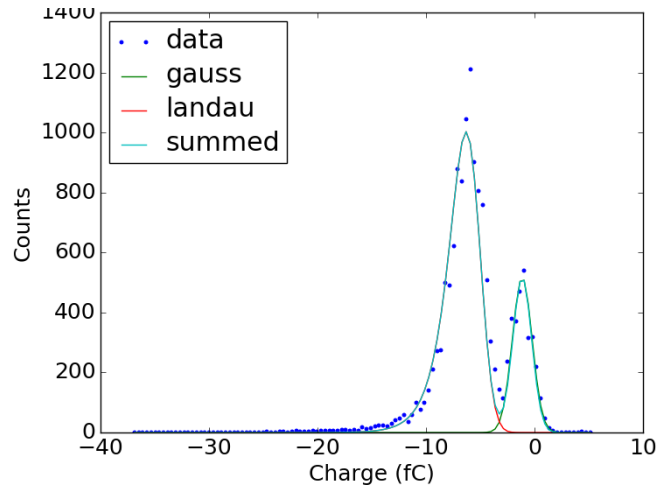


Figure 4.5: The histogram from CCE measurements using the well-studied silicon sensor with superimposed Landau and Gaussian fits to find the gain for the 4150ns collection time, with most probable value in the landau distribution shifted to the left 10%

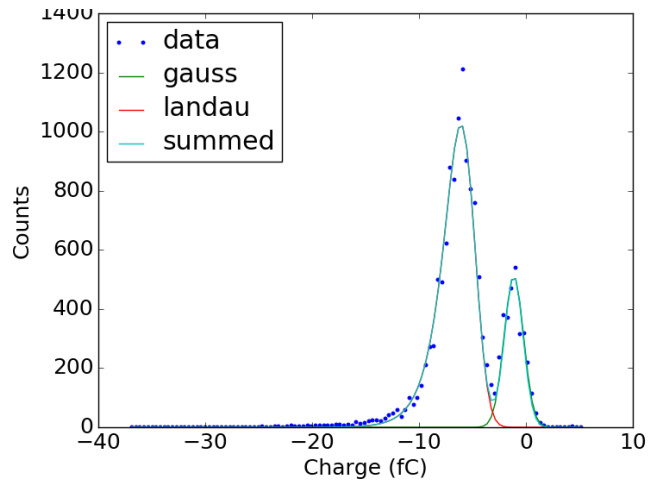


Figure 4.6: The histogram from CCE measurements using the well-studied silicon sensor with superimposed Landau and Gaussian fits to find the gain for the 4150ns collection time, with most probable value in the landau distribution shifted to the left 5%

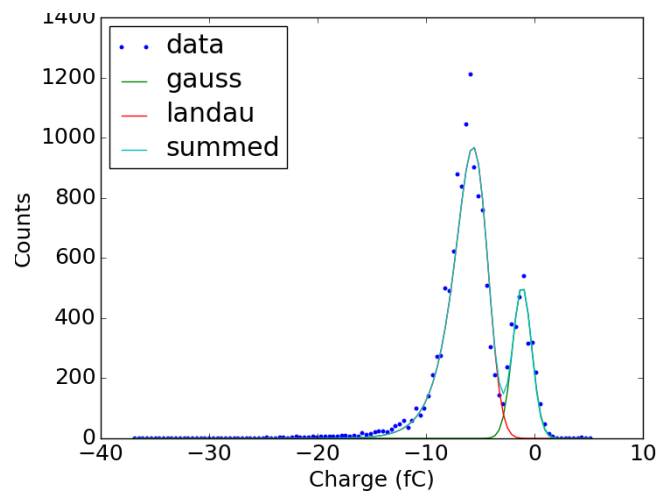


Figure 4.7: The histogram from CCE measurements using the well-studied silicon sensor with superimposed Landau and Gaussian fits to find the gain for the 4150ns collection time, with most probable value in the landau distribution shifted to the right 5%

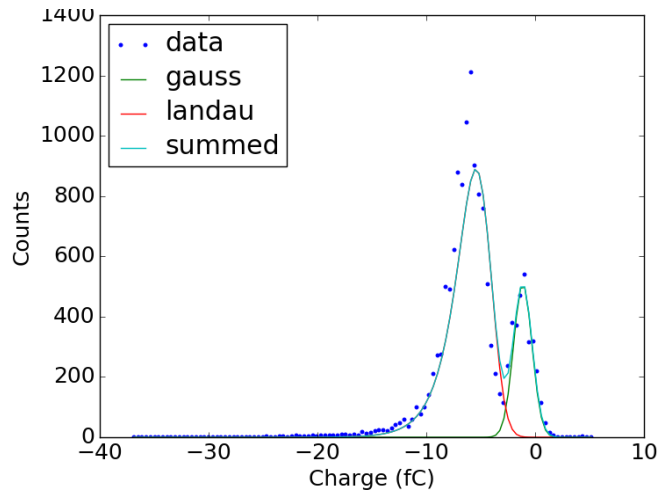


Figure 4.8: The histogram from CCE measurements using the well-studied silicon sensor with superimposed Landau and Gaussian fits to find the gain for the 4150ns collection time, with most probable value in the landau distribution shifted to the right 10%

As we can see, figures 4.5 and 4.6 (the 10% shift) are shifted too much to be considered reasonable fits for the data. Even for figures 4.7 and 4.8 (the 5% shift) the fits seem inconsistent with the data. Instead it was decided that a 4% shift for the most probably value was a better estimate of the uncertainty. We then noted that a 4% uncertainty in the most probable value of the landau led to a 3% error on the measurement. Similar results were found for all six of the collection configurations and so the uncertainty on all the calibrations was assigned to be 3% as seen in table 4.1.

The same technique was used to estimate the uncertainty on the WSI-P4 data; this will be seen in more detail below.

5

Analysis of WSI-P4 Charge Collection

5.1 CCE with WSI-P4

After the gains were found, median charge as a function of collection time could be taken to with the WSI-P4 sensor. The WSI-P4 was placed in the CCE position of the apparatus, the freezer was cooled down to $30^{\circ}\text{C} \pm 1^{\circ}\text{C}$, and CCE data was taken for each collection time at a bias of -800V . The temperature and bias voltage were kept consistent in order to allow a consistent comparison across the range of collection times.

5.2 Results

Table 5.1 shows the median voltage of the observed WSI-P4 sensor singla for each collection time. Also shown is the gain for each collection time, which is just a repeat of Table 4.1. The median voltage is multiplied by the gain resulting in the median collected charge in the final column. Figure 5.1 and 5.2 are graphs of the collection time vs median charge data reported in table 5.1.

Table 5.1: Median Voltages and Charges and their associated gains for given collection times

Collection Time (ns)	Median Voltage(mV)	Gain(mV/fC)	Median Charge (fC)
64	$6.11 \pm 8\%$	$2.06 \pm 3\%$	$2.97 \pm 8.5\%$
120	$11.6 \pm 5\%$	$3.62 \pm 3\%$	$3.20 \pm 6.0\%$
340	$34.5 \pm 3.2\%$	$11.3 \pm 3\%$	$3.05 \pm 4\%$
630	$9.62 \pm 3.2\%$	$3.20 \pm 3\%$	$3.01 \pm 4\%$
1080	$37.0 \pm 3.2\%$	$12.2 \pm 3\%$	$3.03 \pm 4\%$
4150	$3.62 \pm 6.5\%$	$1.04 \pm 3\%$	$3.48 \pm 7\%$

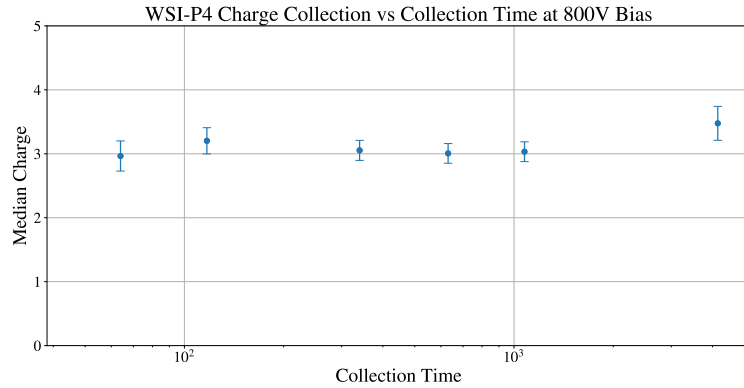


Figure 5.1: Median charges for given collection times for the WSI-P4 data on a x-log plot

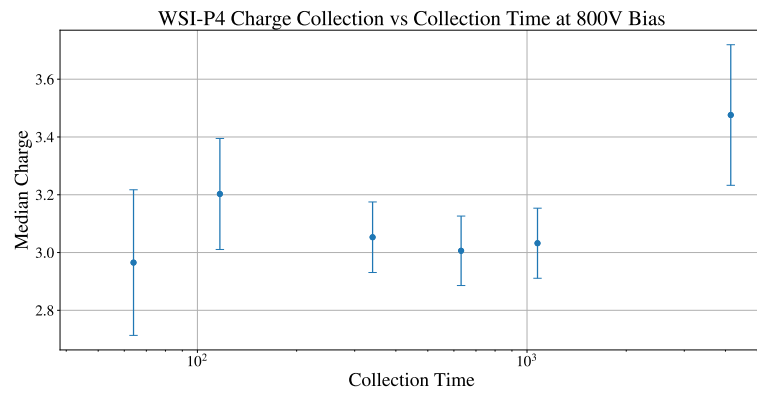


Figure 5.2: Median charges for given collection times for the WSI-P4 data on an x-log plot with the y axis scaled up in order to see the data points and error bars more clearly.

As seen in the table and graphs, the median charge for the first four collection times all agree with each other. We can see there is no significant loss in median charge between these collection times, even at the smallest collection time of 64ns. Each median charge value for those four points is well within the error of the other points. This is what is expected if there is no contributions from trapped and subsequently released charges between the collection time. The outlier in this data set is the largest collection time, 4150ns. This collection time has a higher median charge than the previous four points, and the error on the measurement only slightly overlaps with the error from the other measurements; see figure 5.2 for a clear visual representation. The higher median charge is possibly indicative of trapped charges contributing to the median charge value, indicating that the trapping time for this sensor could be on the order of microseconds. It is difficult to definitively state this given that the difference between the median charge of the 4150ns collection time and the other collection times is only a little larger than the measurement error.

5.3 Error Analysis

Error analysis was performed the same way it was for the gain, described in section 4.3. The error for the smallest and largest collection times were higher than the rest because the signal-to-noise ratio was much lower for those collection times. What causes this phenomena is still unknown and requires further testing.

The collection time with the worst signal-to-noise ratio, and the one with the

largest relative error was the smallest collection time, 64ns. Figures 5.3-5.5 show the nominal fit for the 64ns collection time, and the fits when the most probable value was shifted by $\pm 10\%$. From this we conclude that the uncertainty on the most probable value was 10%, resulting in an 8% error on the median charge. This error was then added in quadrature with the 3% error on the gain calculation, resulting in an overall error of 8.5%. This analysis was done for all the collection times, the results of which can be seen in table 5.1.

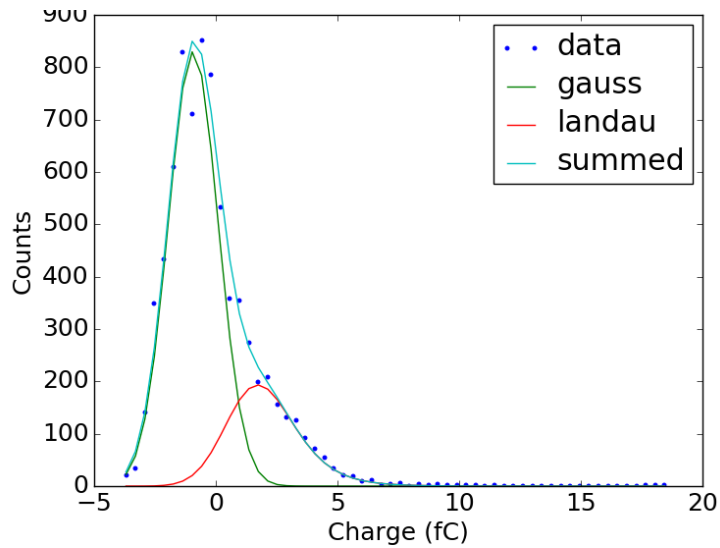


Figure 5.3: Histogram of nominal landau fit of WSI-P4 at 800V for the 64ns collection time

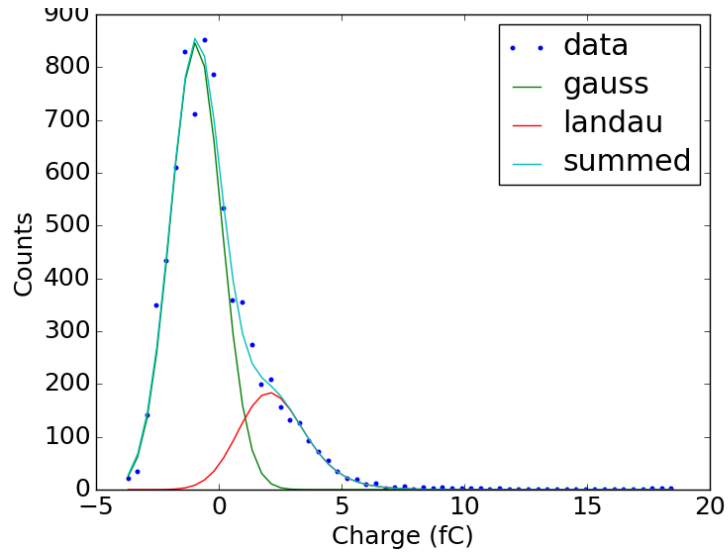


Figure 5.4: Landau and Gaussian fits of WSI-P4 sensor for the 64ns collection time with most probable value in the landau distribution shifted to the left 10%

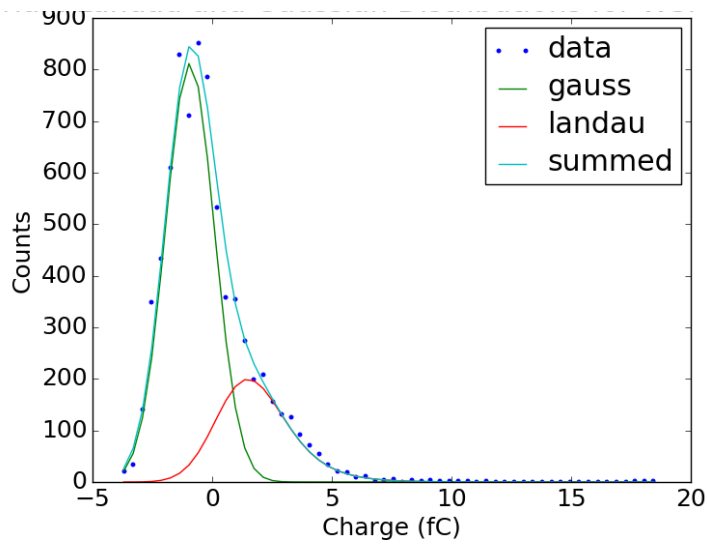


Figure 5.5: Landau and Gaussian fits of WSI-P4 sensor for the 64ns collection time with most probable value in the landau distribution shifted to the right 10%

6

Conclusion

By studying charge collection vs collection time of an irradiated p-type Si sensor we found no clear demonstration of the trap release effect, however there is some indication that the trapping time for the WSI-P4 sensor may be on the order of microseconds. In order to confirm this more collection times between $1\mu\text{s}$ and $4\mu\text{s}$ should be explored to see if there is an upwards trend in median charge between those points.

A large roadblock in analyzing the data presented in this thesis was the small signal to noise ratio for the smaller and larger collection times. The high error in these measurements, especially the largest collection time, prevented us from definitely stating whether there was higher charge collection for longer collection time. So an investigation into the low signal noise ratio is crucial to improving this study.

In the future, more collection times should be investigated. Collection times between 1080ns and 4150ns should be explored to see if there is a trend of increased

median charge. If the high signal to noise issue can be resolved, then pushing the limits of the smallest and largest collection time would be an interesting next step. We could see at what point there is loss in median charge for the shortest collection time, and at what point a higher median charge plateaus for larger collection times.

As far as ILC design, this study has little effect. Even if we are observing higher median charge for collection times on the order of a few microseconds, the median charge is not significantly larger than smaller collection times. Therefore, our conclusions about the CCE of irradiated silicon will not have a strong significance on the design of the electronics in the ILC.

7

Bibliography

Anderson, P et al (2017). Updated Results of a Solid-State Sensor Irradiation Study for ILC Extreme Forward Calorimetry, Proceedings of the LCWS2016 International Workshop on Linear Colliders, Morioka City, Iwate, Japan, December 5–9.

Anderson, P et al (2017). Development of pulse simulations to understand the dependence of collection time on shaping time and explore solutions to the trapping mechanism. University of California, Santa Cruz.

ATLAS Inner Detector Community (1997). ATLAS Inner Detector Volume I Technical Design Report, CERN p 270

Behnke, Ties et al (2007). International Linear Collider Reference Design Report ILC, Volume 1-Summary. Global Design Effort and World Wide Study, 209

Brau, James et al (2007). International Linear Collider Reference Design Report ILC, Volume 4-Detectors. Global Design Effort and World Wide Study, 209

Chisaka, Haruo (1973). Radiation Damage Effects on Silicon Surface Barrier Nuclear Detectors. Japanese Journal of Applied Physics, Vol 12, No. 3.

Erickson, Roger et al (1984). SLC Design Handbook, Stanford Linear Accelerator Center Stanford University, DOE, p 207.

Fabjan, Christian W. and Gianotti, Fabiola (2003). Calorimetry for Particle Physics , Reviews Of Modern Physics, Volume 75, p44.

Fink, Caleb (2016), Design And Implementation Of Readout Instrumentation For Charge Collection Efficiency Measurements Of Solid State Particle Sensors. University of California, Santa Cruz.

Fleischer, R. L. et al (1964). Fission-Track Ages and Track-Annealing Behavior of Some Micas. Science AAAS, p 4.

Junkes , Alexandra (2011), Influence of radiation induced defect clusters on silicon particle detectors. Hamburg University, 210

Matthews, John et al (1996). Bulk radiation damage in silicon detectors and implications for LHC experiments. Nuclear Instruments and Methods in Physics Research, Volume 381, Issue 2-3, p 338-348.

Renteria, CG (2016). Statistical Analysis of Median Charge Deposition for Small-Signal Applications. University of California, Santa Cruz. Richter, B. et al (1980).

SLAC Linear Collider Conceptual Design Report SLAC-229, National Technical Information Service, DOE, p 196.

Weiglein, G (2005). The LHC and the ILC. International Linear Collider Workshop, University of Durham, 10